Title
Comparing Cycling Characteristics of Symmetric Lithium-Polymer-Lithium Cells with Theoretical Predictions

Journal
Journal of The Electrochemical Society, 165(13)

ISSN
0013-4651

Authors
Pesko, Danielle M
Feng, Zhange
Sawhney, Simar
et al.

Publication Date
2018

DOI
10.1149/2.0921813jes

Peer reviewed

Comparing Cycling Characteristics of Symmetric Lithium-Polymer-Lithium Cells with Theoretical Predictions

Danielle M. Pesko,[a,b] Zhange Feng,[c] Simar Sawhney,[a] John Newman,[a,e] Venkat Srinivasan,[c,d] Nitash P. Balsara[a,b,d,e]*

[a] *Department of Chemical and Biomolecular Engineering, University of California, Berkeley, California 94720, USA*

[b] *Materials Sciences Division, Lawrence Berkeley National Laboratory, Berkeley, California 94720, USA*

[c] *Argonne Collaborative Center for Energy Storage Science, Argonne National Laboratory, Lemont, Illinois 60439, USA*

[d] *Joint Center for Energy Storage Research (JCESR), Lawrence Berkeley National Laboratory, Berkeley, California 94720, USA*

[e] *Energy Storage and Distributed Resources Division, Lawrence Berkeley National Laboratory, Berkeley, California 94720, USA*

Abstract

We develop a model based on concentrated solution theory for predicting the cycling characteristics of a lithium-polymer-lithium symmetric cell containing an electrolyte with known transport properties. The electrolytes used in this study are mixtures of polyethylene oxide (PEO) and lithium bis(trifluoromethanesulfonyl) imide (LiTFSI) salt, prepared over a wide range of salt concentrations. The transport properties of PEO/LiTFSI previously reported in the literature are used as inputs for our model. We calculate salt concentration and potential profiles, which develop in these electrolytes under a constant dc polarization, as a function of current density, electrolyte thickness, and salt concentration. These profiles are nonlinear at steady-state due to the strong concentration dependence of the transport properties of this electrolyte. The effect of this nonlinearity on limiting current is demonstrated. Cycling characteristics of a series of lithium symmetric cells were measured to test the validity of our model, without resorting to any adjustable parameters. The time-dependence and steady-state value of the potential measured during cycling experiments were in excellent agreement with model predictions.

Introduction

Next-generation lithium batteries with high energy densities are desired for applications such as electric vehicles and personal electronics. The implementation of these batteries hinges upon the development of novel electrolyte materials with both stability against the lithium metal anode and excellent transport properties. The efficacy of newly-developed electrolytes is usually established in symmetric lithium-electrolyte-lithium cells. In a typical experiment, the cell is polarized in one direction using a constant dc current for a predetermined amount of time, and then the polarization direction is switched. Numerous researchers have reported cycling data from such experiments using potential versus time plots, with an emphasis on the total number of cycles that could be sustained before failure.[1–6] Little attention has been paid to the time-dependence of the cycling profile and the steady-state potential attained at a given current density. While the necessary equations for predicting the cycling behavior of symmetric cells are well established in the concentrated solution theory of Newman,[7,8] we are not aware of any comparisons of these predictions with experimental data. Most of the comparisons between the Newman approach and experimental data focus on cells with porous electrodes and require adjustable parameters or simplifying assumptions.[9–13]

Polymer electrolytes have been identified as promising candidates for lithium metal batteries.[14–17] They are also convenient model systems for measurement of transport coefficients. Ion transport in electrolytes is

governed by three transport coefficients: conductivity, σ, the salt diffusion coefficient, D, and the transference number, t_+.[7] In addition, modeling these systems requires knowledge of the thermodynamic factor, $(1+d\ln\gamma_\pm/d\ln m)$, which quantifies the change in the mean molal activity coefficient of the salt, $\gamma_\pm$, with the molality, m, of the solution. We note in passing that measuring these four parameters in conventional liquid electrolytes is complicated due to convection;[18–20] convection is suppressed in polymers due to high viscosity.

Figure 1 shows the cycling profiles of lithium symmetric cells containing polymer electrolytes that differ in salt concentration. Our electrolytes are comprised of mixtures of polyethylene oxide (PEO) and lithium bis(trifluoromethanesulfonyl) imide (LiTFSI) salt. We use r_{av} to denote the average salt concentration of the electrolyte, where r_{av} is defined as the molar ratio of lithium ions to ether oxygens in the system: $r_{av} = [Li^+]/[O]$. Although both cells in Figure 1 were cycled at the same current density of $i_{ss} = \pm 0.02$ mA/cm^2, the cell containing an electrolyte with a lower salt concentration ($r_{av} = 0.02$) reaches a much lower potential at steady-state compared to the cell with the higher concentration electrolyte ($r_{av} = 0.14$). The concentration-dependence of σ, D, t_+, and $(1+d\ln\gamma_\pm/d\ln m)$ of this PEO/LiTFSI electrolyte have been previously reported.[21,22] At $r_{av} = 0.02$, the ionic conductivity is $\sigma = 7.5 \times 10^{-4}$ S/cm, while at $r_{av} = 0.14$ it is $\sigma = 9.9 \times 10^{-4}$ S/cm. If conductivity were the only relevant transport parameter, then the steady-state potential would be lower for the $r_{av} = 0.02$ cell. Figure 1 shows

that this is clearly not the case. The theoretical work presented in this paper resolves this issue.

Our objective is to compare cycling data of the type presented in Figure 1 with theoretical predictions based on concentrated solution theory. Our theory enables calculation of both potential gradients and salt concentration profiles in an electrolyte at steady-state with no adjustable parameters. It also addresses the time-dependence and steady-state value of potential as a function of applied current.

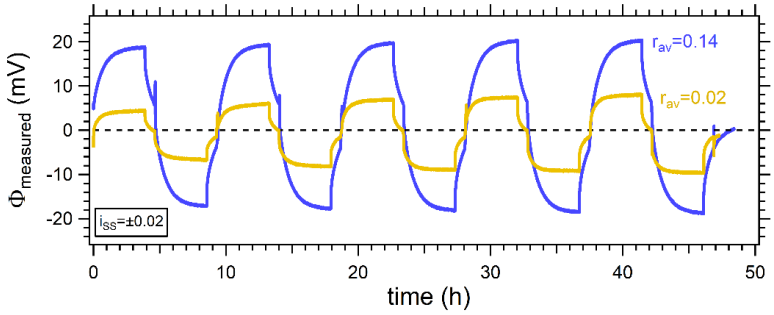

Figure 1. Cycling profiles showing measured potential, $\Phi_{measured}$, as a function of time for lithium-polymer-lithium symmetric cells with PEO/LiTFSI electrolytes at two different salt concentrations. The cells were cycled at a constant current density of i_{ss} = ±0.02 mA/cm^2, and the thicknesses of the electrolytes were approximately 500 µm.

Theory

We use concentrated solution theory[7] to model a cell containing a binary electrolyte wherein the cation is produced at the anode and consumed at the cathode in response to an applied potential, and both the anion and solvent do not participate in the redox reactions. The current is applied in the x-direction across a symmetric cell containing a salt ¿¿ with electrodes of pure metal M. The applied current creates gradients in the salt concentration and the potential across the electrolyte. The reference electrode used to measure the potential at any position in the electrolyte follows the reaction

$$-M^{z+¿+M_{|s|}} \rightleftharpoons ne^{-¿,¿}¿ \quad (0)$$

The anode is located at $x = 0$ and the cathode at $x = L$, where L is the thickness of the electrolyte. We take the potential at the cathode to be zero, and surface overpotentials are taken to be zero at both electrodes.

Steady-State Model

The relationship between the anion flux, N_-, and the current density, i, is given by

$$N_{-¿=-\frac{Dc_T c v_{-¿}}{RTc_0 v}\frac{d\mu_e}{dx}+i\frac{t_{-¿}}{z_{-¿F}},¿¿¿} \quad (0)$$

where D is the diffusion coefficient of the salt based on a thermodynamic driving force, μ_e is the chemical potential of the electrolyte, t_- is the anion transference number ($t_- = 1 - t_+$), and F is Faraday's constant. The concentration terms are c_0, c, and c_T, where c_0 is the solvent concentration, c

117is the salt concentration, and c_T is the total solution concentration ($c_T = c_0 +$
118νc).

119 At steady-state, the net flux of the anion is zero at all values of x. In
120this case, eq. 2 reduces to the following expression in terms of i_{ss}, the
121steady-state current.

$$\frac{d\mu_e}{dx} = i_{ss} \frac{t_{-¿}}{z_{-¿}F \frac{RTc_0\nu}{Dc_T c \nu_{-¿}¿}} ¿ \qquad (0)$$

122The chemical potential of the electrolyte is defined in terms of the molality of
123the solution,

$$\mu_e = \mu_e^0 + \nu RT \ln(m\gamma_\pm) + RT \ln ¿¿ \qquad (0)$$

124where μ_e^0 is the chemical potential of the reference state and $\gamma_\pm$ is the mean
125molal activity coefficient of the electrolyte. Combining eq. 3 and 4, we get

$$\frac{d\mu_e}{dx} = \frac{\nu RT}{m}\left(1 + \frac{d\ln\gamma_\pm}{d\ln m}\right)\frac{dm}{dx} = i_{ss} \frac{t_{-¿}}{z_{-¿}F \frac{RTc_0\nu}{Dc_T c \nu_{-¿}.¿}} ¿ \qquad (0)$$

126The salt diffusion coefficient D measured in a restricted diffusion experiment
127is based on the relaxation of a concentration gradient and is related to D by

$$D = D\frac{c_T}{c_0}\left(1 + \frac{d\ln\gamma_\pm}{d\ln m}\right). \qquad (0)$$

128 In this work, we prefer to describe salt concentration in terms of r, the
129molar ratio of lithium ions to ether oxygens in the system. Given that r =
130mM_0, where M_0 is the molar mass of the solvent, it is straightforward to

convert from m to r in these equations. Combining eq. 5 and 6 and performing this conversion, we get

$$\frac{dr}{dx} = \frac{i_{ss}}{Fz \left(-\nu_{-} r \frac{t_{-}(r)}{D(r)c(r)} \right)} \quad (0)$$

Collecting the r-dependent terms and integrating over them gives an implicit expression for the concentration profile, $r(x)$, for a given $r(x=0)$ and $i_{ss}L$.

$$\int_{r(x=0)}^{r(x)} \frac{D(r)c(r)}{r\, t_{-}(r)} dr = \frac{i_{ss} L}{Fz \left(-\nu_{-} \left(\frac{x}{L} \right) \right)} \quad (0)$$

In an experiment one controls the average concentration of the electrolyte, r_{av}, which is obtained by integrating $r(x)$ from $x = 0$ to $x = L$. The spatial dependence of the molar salt concentration, $c(x)$, can then be readily obtained from $r(x)$ as long as the concentration-dependence of the density of the electrolytes is known.

The potential gradient $d\Phi/dx$ in the cell can be determined for a given current density using the relationship

$$i = -\sigma \frac{d\Phi}{dx} - \frac{\sigma}{F} \quad (0)$$

where σ is the conductivity of the electrolyte and t_+ is the cation transference number. Since the electrolyte is electrically neutral, μ_e depends only on local concentration, and is independent of Φ. Charge balance implies that $z_+ = n$. Eq. 9 applies to both steady-state wherein both terms on the right contribute and the initial state wherein the second term on the right is zero because the solution is initially uniform in concentration. At the initial

148state, dΦ/dx will be constant. Thus, the initial current density, i_0, at t = 0 is
149related to the initial potential, Φ_0, by

$$i_0 = \sigma \frac{\Phi_0}{L}. \quad (0)$$

150The relationship between the current density and potential at steady-state is
151given by combining eq. 3, 6, and 9,

$$i_{SS} = -\sigma \frac{d\Phi_{SS}}{dx} - i_{ss} Ne, \quad (0)$$

152where Ne is given by[23]

$$Ne = \frac{v}{¿¿¿} \quad (0)$$

153The parameter Ne can be measured by a steady-state current experiment
154and is related to the quantity i_{ss}/i_0, often referred to as the steady-state
155current transference number, $t_{+,SS}$.

$$t_{+,SS} = \frac{i_{ss}}{i_0} = \frac{1}{1+Ne}. \quad (0)$$

156Eq. 11 can be integrated to obtain the spatial dependence of potential,

$$\Phi_{SS}(x) = -Fz_{-¿v} \int_{-¿}^{r|x|} \frac{D|r|c|r|}{r t_{+,SS}|r|\sigma|r|t_{-|r|}} dr.¿¿ \quad (0)$$

157where dr/dx determined above is used. Thus, prediction of Φ_{ss} across an
158electrolyte using eq. 14 requires knowledge of the concentration-
159dependence of three independent transport properties, σ, D, and t_-, in
160addition to $t_{+,ss}$ and c.

161*Transient Model*

162 For unsteady-state problems, it is customary to start with eq. 12.14
163from reference 7 which describes the mass transport of the salt in the

electrolyte based on concentrated solution theory. This relationship, simplified to one-dimensional transport along the *x*-direction in the absence of convection, is given by

$$\frac{\partial c}{\partial t}=\frac{\partial}{\partial x}\left[D\left(1-\frac{d\ln c_0}{d\ln c}\right)\frac{\partial c}{\partial x}\right]-\frac{i_{ss}}{z_{+¿}\nu_{+¿F}¿¿¿} \quad (0)$$

with boundary conditions

$$-D\left.\frac{dc}{dx}\right|_{x=0}=1-\frac{t_{+¿}}{F}i_{ss}¿ \quad (0)$$

$$-D\left.\frac{dc}{dx}\right|_{x=L}=-1-\frac{t_{+¿}}{F}i_{ss}.¿ \quad (0)$$

Equation 15 can be solved numerically to obtain transient concentration profiles, $c(x,t)$, across an electrolyte.

In order to obtain transient potential profiles, $\Phi(x,t)$, across an electrolyte, we use the relationship between i_{ss} and Φ given by a modified Ohm's law that includes the overpotential due to concentration gradients in the electrolyte.

$$i_{ss}=-\sigma\frac{d\Phi}{dx}-\frac{2\sigma RT}{F}\left(1+\frac{d\ln f_{\pm}}{d\ln c}\right)¿ \quad (0)$$

Equation 18 is solved numerically with Butler-Volmer kinetics used to account for the charge-transfer reaction at the electrode boundaries.

$$i_{ss}|_{x=0}=i_e\left[\exp\left(\frac{\alpha_a F}{RT}\left(\Phi_1-\Phi(x=0)\right)\right)-\exp\left(\frac{-\alpha_c F}{RT}\left(\Phi_1-\Phi(x=0)\right)\right)\right] \quad (0)$$

$$i_{ss}|_{x=L} = i_e\left[\exp\left(\frac{-\alpha_a F}{RT}\Phi(x=L)\right) - \exp\left(\frac{\alpha_c F}{RT}\Phi(x=L)\right)\right] \quad (0)$$

Here, i_e is the exchange current density, and α_a and α_c are the anodic and cathodic transfer coefficients, respectively. The electrode potential at $x = 0$ is Φ_1. The parameters used in our unsteady-state model are: $\alpha_a = \alpha_c = 0.5$, and $i_0 = 0.5$ mA/cm^2, based on previous work on a closely related system.[24] Under these conditions, the difference between the electrode potential and that in the electrolyte at $x = L$ are negligible.

At steady-state dc/dt = 0, and eq. 15 simplifies to

$$D\left(1 - \frac{d\ln c_0}{d\ln c}\right)\frac{dc}{dx} = i_{ss}\frac{t_{+¿}}{z_{+¿}v_{+¿F}+K.¿}¿ \quad (0)$$

The constant K is determined using the condition dc/dx = 0 when $t_+ = 1$. This gives

$$D\left(1 - \frac{d\ln c_0}{d\ln c}\right)\frac{dc}{dx} = \frac{-i_{ss}}{z_{+¿}v_{+¿F}¿¿}¿ \quad (0)$$

Collecting the concentration-dependent terms and integrating gives

$$\int_{c(x=0)}^{c(x)} \frac{D(c)}{t_{-¿(c)}\left(1 - \frac{d\ln c_0}{d\ln c}\right)}dc = \frac{-i_{ss}L}{z_{+¿}v_{+¿F}\left(\frac{x}{L}\right).¿}¿ \quad (0)$$

Eq. 23 is formally equivalent to eq. 8 due to the interrelations between c, r, and c_0.

Methods

Experiment – Cell Preparation and Cycling

All sample preparation was performed inside an argon glovebox (MBraun) in order to maintain water and oxygen levels below 1 and 5 ppm, respectively. Electrolytes were prepared by mixing PEO purchased from PolymerSource (5 kg/mol with a polydispersity of 1.08) with LiTFSI salt purchased from Novolyte. The polymers were dried at 90°C under vacuum in the glovebox antechamber for 24 h. The salt was dried at 120°C under vacuum in the glovebox antechamber for 3 days. Electrolytes were prepared by dissolving dry polymer and LiTFSI salt into tetrahydrofuran (THF) at 55°C until completely dissolved. The THF was evaporated, leaving behind a polymer/salt mixture. After 12 hours of drying on the hot plate at 55°C, the electrolytes were transferred to the glovebox antechamber to dry under vacuum at 90°C for 24 h to remove any excess THF. The average salt concentration in the electrolyte is described as r_{av}, the molar ratio of lithium ions to ether oxygens on the polymer: $r_{av} = [Li^+]/[O]$. Electrolytes were prepared in a wide range of salt concentrations of $0.01 \leq r_{av} \leq 0.30$.

Lithium symmetric cells were assembled by pressing the polymer electrolyte into a silicone spacer with a diameter of 3.175 mm and a thickness of 508 µm. The electrolyte was then sandwiched between two 150 µm thick lithium foils (MTI Corporation) backed with nickel foil. A stainless-steel shim was placed on either side of the sample to prevent the sample from deforming, which could lead to a change in electrolyte thickness or a

cell short. Nickel tabs were secured to the stainless-steel shims to serve as electrical contacts. The assembly was vacuum sealed in a laminated aluminum pouch material (Showa-Denko) before removal from the glovebox. All samples were annealed at 90°C for 4 hours prior to electrochemical characterization.

Cycling was performed using a Biologic VMP3 potentiostat, and the cells were maintained at 90°C using a home-built heating stage. Cells were polarized at a low current density of i_{ss} = 0.02 mA/cm^2, and the potential, $\Phi_{measured}$, was recorded as a function of time for five charge/discharge cycles. Each cycle consisted of a 4 h charge, 45 min rest, 4 h discharge, and 45 min rest. Examples of cycling data ($\Phi_{measured}$ vs. t) obtained from lithium symmetric cells with electrolytes of different salt concentrations are shown in Figure 1. Between each cycle, ac impedance spectroscopy was performed to track the cell impedance as a function of time. For each of these measurements, complex impedance was acquired for a frequency range of 1 MHz to 100 mHz at an amplitude of 80 mV. The data were analyzed in the form of a Nyquist plot and fit to an equivalent electrical circuit suitable for a symmetric cell with nonblocking electrodes to obtain R_i, the interfacial resistance of the cell, as described in previous publications.[21,25] The value of R_i taken immediately subsequent to a given charge/discharge measurement is used to correct $\Phi_{measured}$ for the potential drop across the interface according to eq. 26.

Cells prepared with an electrolyte concentration of r_{av} = 0.18 were cycled at higher current densities following the initial five cycles at i_{ss} = 0.02 mA/cm^2. In this case, one full charge/discharge cycle was performed at each of the following current densities: i_{ss} = 0.05, 0.09, 0.12, 0.15, 0.20, and 0.25 mA/cm^2.

After the cycling experiments were completed, the cells were disassembled in the glovebox, and the final electrolyte thickness, L, was measured using a micrometer. These values are used in our analysis to normalize the potential of each cell according to thickness.

Transient Model – Comsol Parameters

The transient model, based on a macro-homogeneous model by Newman and coworkers,[10,26,27] is used to calculate the time-dependence of the potential across a lithium-PEO/LiTFSI-lithium symmetric cell during dc polarization. The governing equations for this model (eq. 15-20), are solved numerically using Comsol 5.3. The exchange current density, i_e, is taken to be 0.5 mA/cm^2, and the anodic and cathodic transfer coefficients, α_a and α_c, are both taken to be 0.5, based on a previous report using similar materials.[24]

To solve these equations, it is necessary to fit each transport property and the thermodynamic factor as continuous functions of salt concentration. The thermodynamic factor used in these equations is $(1+d\ln f_{\pm}/d\ln c)$, which quantifies the change in the mean molar activity of the salt, $f_{\pm}$, with the molarity, c, of the solution; this parameter is different from $(1+d\ln \gamma_{\pm}/d\ln m)$, which is based on the molality of the solution. The polynomial expression used for fitting and the results thus obtained are given in Table 1.

Table 1. Fitting parameters used for each transport and thermodynamic property used in the Comsol modeling. All parameters, P, are given as functions of concentration, c, in mol/L. Units for conductivity are S/cm and diffusion are cm^2/s. Most parameters were broken up into two concentration ranges to obtain the most accurate fits.

$$P(c) = K_0 + K_1 c + K_2 c^2 + K_3 c^3 + K_4 c^4 + K_5 c^5$$

P(c)	***range***	***K_0***	***K_1***	***K_2***	***K_3***	***K_4***	***K_5***
σ	$c \leq 2.58$	2.53×10^{-4}	-1.48×10^{-3}	7.73×10^{-3}	-5.69×10^{-3}	1.16×10^{-3}	-
	$c > 2.58$	-7.26×10^{-2}	7.13×10^{-2}	-2.24×10^{-2}	2.29×10^{-3}	-	-

D	$c \leq 2.38$ $c > 2.38$	6.92×10^{-8} -7.87×10^{-5}	-1.04×10^{-7} 1.21×10^{-4}	3.51×10^{-7} -7.31×10^{-5}	-2.50×10^{-7} 2.19×10^{-5}	4.93×10^{-8} -3.24×10^{-6}	-1.90×10^{-7}
t_+	$c \leq 2.58$ $c > 2.58$	-8.95×10^{-2} -68.2	0.768 59.9	-0.258 -17.2	-3.08×10^{-2} 1.63	- -	- -
$\left(1+\frac{d\ln f_{\pm}}{d\ln c}\right)$	$c \leq 2.58$ $c > 2.58$	3.34×10^{-3} -352	0.857 295	2.23 -78.8	-0.785 6.85	- -	- -
$\left(1-\frac{d\ln c_0}{d\ln c}\right)$	*all c*	0.964	-0.108	-2.94×10^{-2}	-	-	-

Results and Discussion

In order to model concentration or potential profiles in an electrolyte, measurements of transport properties (conductivity, σ, salt diffusion coefficient, D, cation transference number, t_+) and the thermodynamic factor, $(1+d\ln\gamma_{\pm}/d\ln m)$, must be obtained over a wide range of salt concentrations.[7] Table 2 shows the transport properties of an electrolyte composed of 5 kg/mol PEO mixed with LiTFSI salt. These measurements have been thoroughly discussed in recent reports from our group.[21,22] Here, salt concentration is defined in two ways: r is the molar ratio of lithium ions to ether oxygens in the system, $r = [Li^+]/[O]$, and c is the molarity of the solution. We have added the steady-state transference number, $t_{+,ss}$, defined by eq. 13 in Table 2 as it convenient for the calculations given below.

Table 2. Transport properties of a 5 kg/mol PEO/LiTFSI electrolyte at 90 ºC.

r	***c*** **(mol/cm³)**	***D*** **(cm²/s)**	***σ*** **(S/cm)**	t_+	**(1+dln*γ*±/dln*m*)**	$t_{+,ss}$
0.01	2.47×10^{-4}	$[6.0 \pm 0.8] \times 10^{-8}$	$[2.7 \pm 0.6] \times 10^{-4}$	0.07 ± 0.02	0.43	0.18 ± 0.009
0.02	4.73×10^{-4}	$[7.8 \pm 0.7] \times 10^{-8}$	$[7.5 \pm 0.4] \times 10^{-4}$	0.23 ± 0.03	0.69	0.16 ± 0.015
0.04	8.71×10^{-4}	$[1.0 \pm 0.1] \times 10^{-7}$	$[1.8 \pm 0.5] \times 10^{-3}$	0.40 ± 0.13	1.70	0.11 ± 0.019

0.06	1.20×10^{-3}	$[1.3 \pm 0.4] \times 10^{-7}$	$[2.0 \pm 0.2] \times 10^{-3}$	0.33 ± 0.11	2.23	0.11 ± 0.005
0.08	1.59×10^{-3}	$[1.1 \pm 0.1] \times 10^{-7}$	$[2.2 \pm 0.8] \times 10^{-3}$	0.43 ± 0.17	3.33	0.10 ± 0.012
0.10	1.87×10^{-3}	$[8.4 \pm 1.1] \times 10^{-8}$	$[1.3 \pm 0.2] \times 10^{-3}$	0.20 ± 0.05	2.82	0.09 ± 0.013
0.12	2.11×10^{-3}	$[7.0 \pm 1.7] \times 10^{-8}$	$[1.1 \pm 0.0] \times 10^{-3}$	0.08 ± 0.02	2.78	0.08 ± 0.008
0.14	2.38×10^{-3}	$[5.8 \pm 0.9] \times 10^{-8}$	$[9.9 \pm 2.3] \times 10^{-4}$	-0.08 ± 0.02	2.66	0.07 ± 0.005
0.16	2.58×10^{-3}	$[9.4 \pm 0.8] \times 10^{-8}$	$[1.3 \pm 0.4] \times 10^{-3}$	-0.38 ± 0.13	2.27	0.06 ± 0.001
0.18	2.76×10^{-3}	$[9.0 \pm 1.0] \times 10^{-8}$	$[1.6 \pm 0.6] \times 10^{-3}$	0.10 ± 0.04	3.74	0.07 ± 0.011
0.21	3.05×10^{-3}	$[6.5 \pm 1.5] \times 10^{-8}$	$[1.2 \pm 0.4] \times 10^{-3}$	0.41 ± 0.16	6.32	0.10 ± 0.006
0.24	3.36×10^{-3}	$[6.3 \pm 1.0] \times 10^{-8}$	$[6.4 \pm 2.4] \times 10^{-4}$	0.33 ± 0.13	6.00	0.16 ± 0.010
0.27	3.49×10^{-3}	$[5.9 \pm 1.3] \times 10^{-8}$	$[4.0 \pm 1.0] \times 10^{-4}$	0.18 ± 0.06	5.24	0.18 ± 0.022
0.30	3.78×10^{-3}	$[4.2 \pm 0.6] \times 10^{-8}$	$[1.5 \pm 0.2] \times 10^{-4}$	-0.02 ± 0.00	4.49	0.26 ± 0.020

To calculate concentration gradients in any system using eq. 8, the transport properties of the electrolyte must be fit as a continuous function of salt concentration. Based on the data in Table 2, we calculate the parameter $(D\ c)/(r\ t_-)$ for our PEO/LiTFSI electrolytes, shown in Figure 2. The anion transference number, t_-, is equal to 1 - t_+. The solid curve shows a least-squares fit to the equation

$$\frac{Dc}{rt_{-} = ar^5 + br^4 + cr^3 + dr^2 + er + f,} \quad (0)$$

with fitting parameters

where D is in cm^2/s and c is in mol/cm^3. Alternatively, one could fit each parameter (D, t_-, c) individually as a function of r. It is important to note that our data are limited to the range $0.01 < r < 0.3$. Thus, our model can only be used to study symmetric cell data wherein the entire salt concentration profile in the cell falls within these bounds.

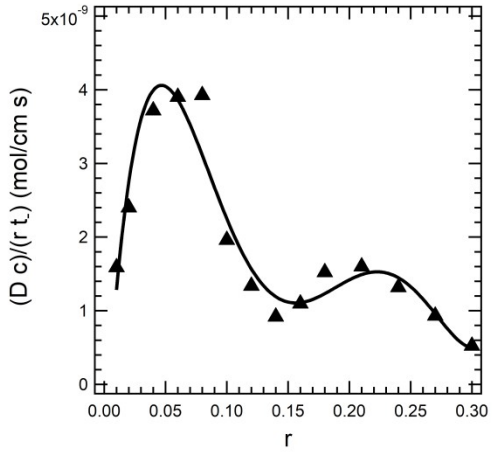

Figure 2. Fit of the transport coefficient term, $(D\ c)/(r\ t_-)$, with LiTFSI salt concentration. The solid curve shows the least-squares polynomial fit given by eq. 24.

The concentration profile in a symmetric cell under steady-state operation is governed by the initial salt concentration of the electrolyte which we call r_{av}, the steady-state current density, i_{ss}, and the thickness of the electrolyte, L. Before the cell is polarized, the salt concentration at all locations is r_{av}. At steady-state, the salt concentration profile is governed by eq. 8; solution to this equation gives the position-dependent salt concentration, $r(x)$. It is convenient to determine the concentration profile as a function of x/L. Calculating the concentration profile for a given value of

the product $i_{ss}L$ requires a three-step iterative process: (1) Choose a value for r at the point $x/L = 0$. (2) Calculate r as a function of x/L from $0 \leq x/L \leq 1$ using eq. 8. (3) Integrate $r(x/L)$ from 0 to 1 to determine the average salt concentration, r_{av}, of the electrolyte. The process is repeated, adjusting the value of r at $x/L = 0$, until the desired r_{av} is reached.

Figure 3 shows salt concentration profiles for PEO/LiTFSI electrolytes with different salt concentrations: $r_{av} = 0.08$, 0.10, 0.12, and 0.14. Each panel corresponds to a different value of $i_{ss}L$. Figure 3 could represent three cells with the same thickness at different current densities (L = 500 μm and (a) i_{ss} = 0.8 mA/cm^2, (b) i_{ss} = 0.2 mA/cm^2, and (c) i_{ss} = 0.02 mA/cm^2) or with different thicknesses at the same current density (i_{ss} = 1 mA/cm^2 and (a) L = 400 μm (b) L = 100 μm and (c) L = 10 μm). At the lowest value of $i_{ss}L$ = 0.001 mA/cm (Figure 3a), the concentration profiles are linear. Nonlinear concentration profiles are evident when $i_{ss}L$ is increased 0.01 mA/cm (Figure 3b). Further increase in $i_{ss}L$ to 0.04 mA/cm results in highly nonlinear concentration profiles (Figure 3c). For the r_{av} = 0.08 electrolyte shown in Figure 3c, $r(x)$ approaches zero at x/L = 1. The minimum value of $r(x/L=1)$ is zero; this condition is defined as the limiting current density of an electrolyte. The nonlinear concentration profiles in Figure 3b and c are due to the concentration-dependence of t_+ and D. If t_+ and D were independent of salt concentration and c were proportional to r, all profiles in Figure 3 would be linear. Interestingly, the concentration profile at a given current density does not depend on conductivity (see eq. 8); the values of the conductivity

only affect the cell potential required to achieve a given current density (see eq. 14).

Equation 7 indicates that the concentration gradient, dr/dx, at a given location, x/L, in the symmetric cell is governed entirely by the local salt concentration, r, regardless of the overall salt concentration, r_{av}, of the electrolyte. Thus, in Figure 3 if one moves horizontally from one curve to the next at any chosen value of r, the gradients of the concentration profiles are identical. At steady-state, the overall flux of cations, given by i_{ss}, is independent of position (x/L). The migration and diffusion components of the flux will change with position due to the concentration dependence of t_+ and D. The slope of the concentration profile changes due to this effect.

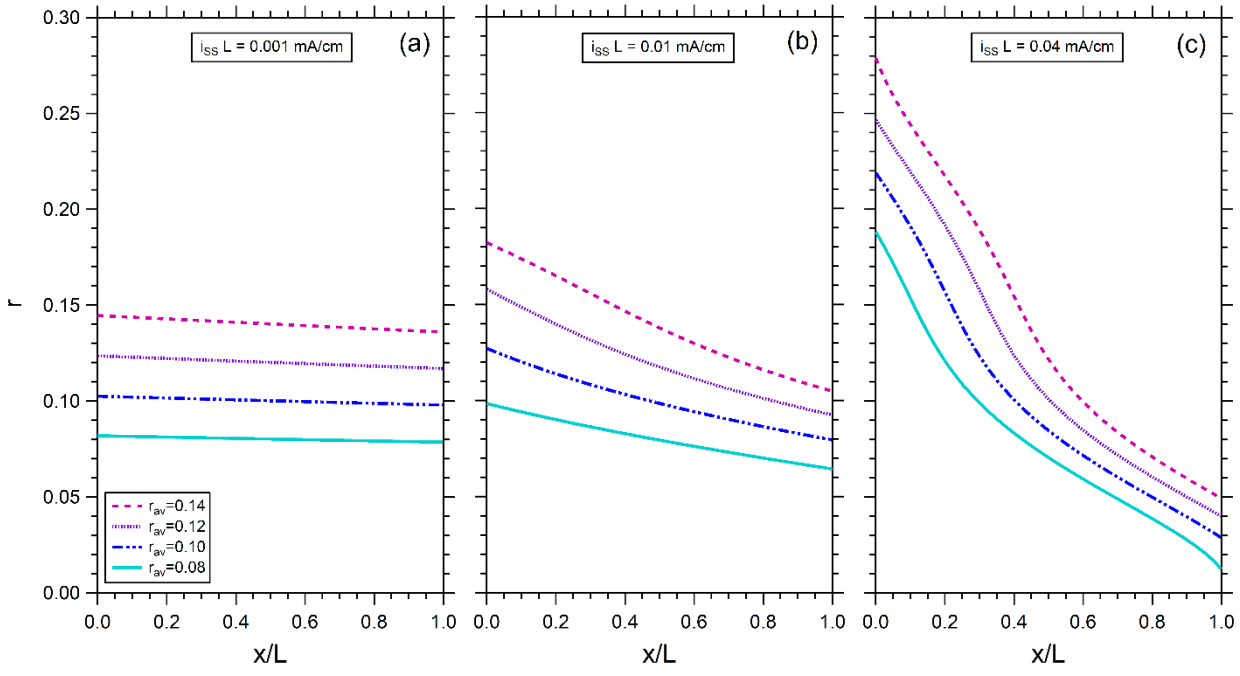

Figure 3. Concentration gradients in PEO/LiTFSI electrolytes predicted by the model at steady-state. These are calculated using eq. 8 based on the fit of the transport parameter in Figure 2.

The limiting current density is an important characteristic of an electrolyte, as it defines the maximum current that can be drawn from a cell during operation. Traditionally, equations used to describe this characteristic are based on the assumption of transport properties that are independent of salt concentration.[7] We use our model to calculate the limiting current density as a function of salt concentration for PEO/LiTFSI electrolytes. The limiting current density, i_{limit}, is defined as the value of i_{ss} when the concentration profile exhibits $r = 0$ at $x/L = 1$. Our expressions for transport properties and the thermodynamic factor were derived from data in the salt concentration range of $0.01 \leq r \leq 0.3$. In other words, $r = 0$ lies outside the parameter window. To overcome this issue, we use our model at a chosen value of r_{av} to obtain r at $x/L = 1$ with increasing i_{ss} up to the limit of $r = 0.01$ at $x/L = 1$. Typical data thus obtained at $r_{av} = 0.08$ are shown in Figure 4a. Extrapolating these data to $r = 0$ gives the value of the limiting current density. Only the product $i_{limit}L$ appears in the governing equation (eq. 8); we thus report on this parameter. Figure 4b shows the product $i_{limit}L$ as a function of r_{av}. It is evident that $i_{limit}L$ exhibits a nonlinear dependence on salt concentration due to the nonlinear concentration profiles observed in these electrolytes.

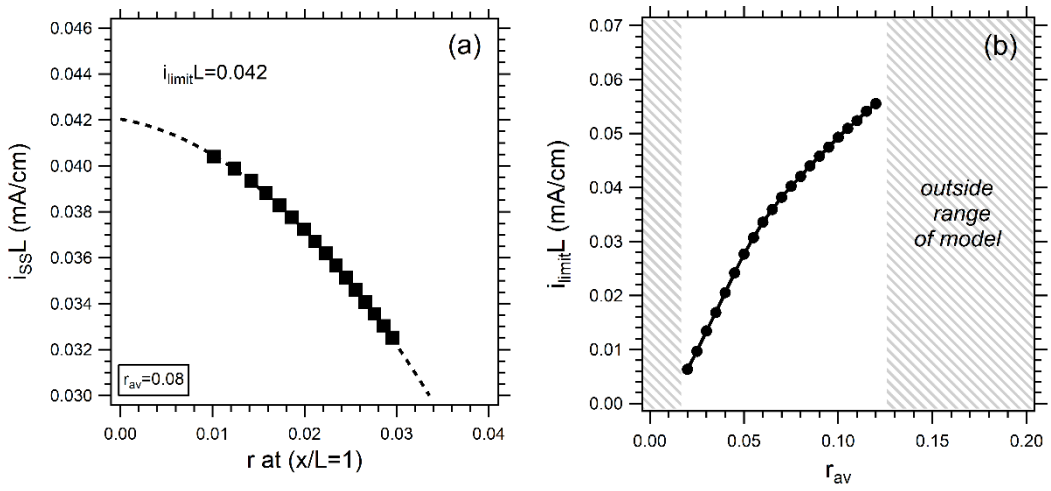

365

366**Figure 4. (a)** Model predictions of $i_{ss}L$ as a function of r at $x/L = 1$ for an electrolyte
367with a salt concentration of $r_{av} = 0.08$. Here, the dotted line shows the least-squares
368polynomial fit, which is used to extrapolate the data to a value of $r = 0$ at $x/L = 1$ to
369obtain the limiting current density (here shown as $i_{limit}L$). **(b)** The product $i_{limit}L$ for
370PEO/LiTFSI predicted by the model as a function of electrolyte salt concentration.
371Our predictions are limited to $0.02 \leq r_{av} \leq 0.12$ due to the limited concentration
372range of the fits used in our model.
373

374 To calculate potential gradients in our electrolytes using eq. 14, we fit
375the transport parameter $(D\ c)/(r\ t_{-}\ \sigma\ t_{+,ss})$ as a continuous function of salt
376concentration, shown in Figure 5. A double exponential gives the most
377precise fit for this data, and is given by

$$\frac{Dc}{rt_{-}\sigma t_{+,ss}} = k_0 + A_1 \exp(-\tau_1 r) + A_2 \exp(-\tau_2 r), \quad (0)$$

378with fitting parameters

379

380where D is in cm^2/s, c is in mol/cm^3, and σ is in S/cm.

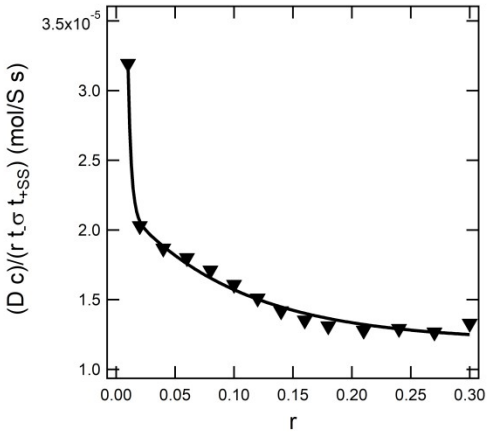

Figure 5. Fit of transport coefficient term $(D\ c)/(r\ t_-\ \sigma\ t_{+,SS})$ with LiTFSI salt concentration. The solid curve shows the least-squares fit to the double exponential given in eq. 25.

Figure 6 shows the dependence of potential, Φ, on position calculated for the electrolytes shown in Figure 3 (r_{av} = 0.08, 0.10, 0.12, and 0.14) at the same three values of $i_{ss}L$. We define Φ = 0 at x/L = 1. At the lowest value of $i_{ss}L$, Φ is a linear function of position (Figure 6a). Nonlinear dependences of Φ on position are evident at higher values of $i_{ss}L$ (Figure 6b and c). There is a close relationship between the nonlinearity in potential seen in Figure 6 and the nonlinearity in concentration seen in Figure 3. In an experiment, the value of cell potential measured experimentally corresponds to Φ at x/L = 0. It is clear that for a given value of $i_{ss}L$, cells prepared with electrolytes of different salt concentrations will yield different values of Φ at steady-state. Interestingly, the cell potential (Φ at x/L = 0) is a stronger function of salt concentration at $i_{ss}L$ = 0.001 mA/cm when compared to $i_{ss}L$ = 0.04 mA/cm (compare inset in Figure 6a with Figure 6c). This is because of the large concentration gradients that are obtained at high values of $i_{ss}L$ (see Figure

4c). The transport parameters of our electrolytes are strong functions of salt concentration, but when large concentration gradients are present in the electrolyte these properties are integrated over a wide concentration window that is not a sensitive function of r_{av}. Next, we examine the validity of our model by comparing theoretical predictions against experimental measurements of Φ.

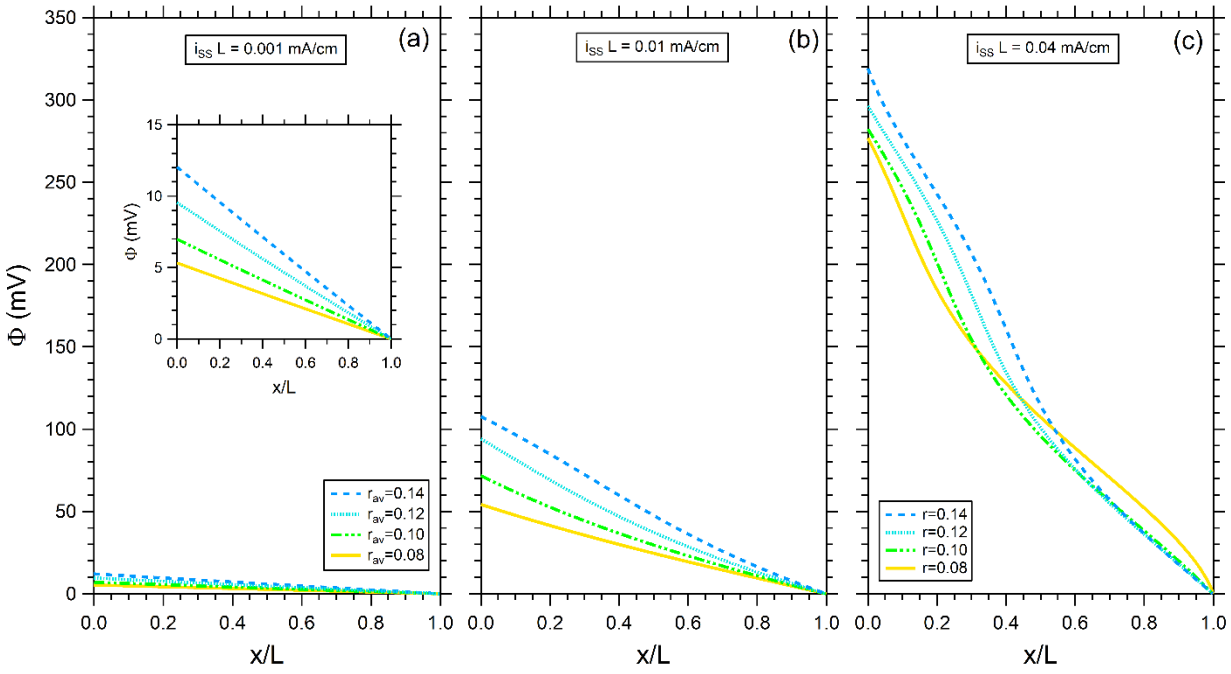

Figure 6. Potential profiles in PEO/LiTFSI electrolytes predicted by the model at steady-state. These are calculated using eq. 14 based on the fit of the transport parameters in Figure 5.

We use the calculations described above to interpret experimental data from lithium symmetric cells with PEO/LiTFSI electrolytes. The cells were cycled at increasing values of i_{ss}, and the measured potential, $\Phi_{measured}$, was recorded as a function of time. Typical time-dependent potential curves thus

obtained are shown in Figure 7a. These data correspond to an electrolyte with $r_{av} = 0.18$ cycled at current densities ranging from $i_{ss} = 0.02$ to $i_{ss} = 0.25$ mA/cm^2. At each current density, the potential increases with time due to the formation of concentration gradients in the electrolyte, and then plateaus as the cell reaches steady-state. The measured potential, $\Phi_{measured}$, cannot be directly compared to Φ predicted by the model, as it has contributions from the lithium-polymer interfaces that are not included in the model. To correct for this, we subtract the potential drop due to interfacial impedance,

$$\Phi(t)=\Phi_{measured}(t)-R_i i_{ss} A, \qquad (0)$$

where R_i is the interfacial resistance obtained from ac impedance and A is the area of the cell. The time-dependent potential curves were obtained after the interfacial impedance had reached a steady value; thus, the product $R_i i_{ss} A$ is taken to be constant at all values of t. For the case of the experimental data, we normalize Φ by the measured thicknesses of the cells, which are in the vicinity of 500 μm. In our comparisons below, all measured potentials are presented after correcting for interfacial impedance and normalizing by thickness (Φ/L). Figure 7b shows the data from Figure 7a with this correction applied.

The relevant metric for direct comparison between the experimental data in Figure 7b and the model based on eq. 14 is the potential obtained at steady-state, Φ_{ss}/L. In Figure 7c we show this comparison for an electrolyte with $r_{av} = 0.18$. The model results were obtained for an electrolyte with $L =$ 500 μm at increasing values of i_{ss}. The experimental measurements

correspond to the same values of i_{ss} shown in Figure 7b; each point represents an average of three samples, and the error bars show the standard deviation. The data in Figure 7c are in good agreement with theoretical predictions at low values of i_{ss}, but deviations are evident at higher values of i_{ss}. The explanation for this may be related to the mechanism of cell failure witnessed in the experimental measurements. Upon cycling at increasing i_{ss}, all three cells failed at $i_{ss} \leq 0.25$ mA/cm^2, which is below the limiting current density predicted by the model. If the experimental samples had reached the limiting current denisty, one might expect the voltage profile to exhibit a spike indicating depletion of the salt at the electrode. Instead, we observe that cell failure is indicated by an unstable voltage that eventually drops to zero ($i_{ss} = 0.25$ mA/cm^2 in Figure 7a and b), pointing to a short circuit in the cell. Given the low modulus of 5 kg/mol PEO at 90ºC, we believe this can be attributed to the formation of lithium dendrites as the cell reaches high current densities, leading to a deviation of Φ_{ss}/L from the model at high i_{ss} and eventually resulting in cell failure. This experimental constraint prevents us from studying our cells at high current densities. We thus limit the rest of our discussion comparing model and experiment to $i_{ss} = 0.02$ mA/cm^2, where we expect dendrites are not affecting our results. At this current density, cell potential is a strong function of r_{av} as shown in the inset Figure 6a ($i_{ss}L = 0.001$ mA/cm corresponds to $i_{ss} = 0.02$ mA/cm^2, as $L = 500$ µm).

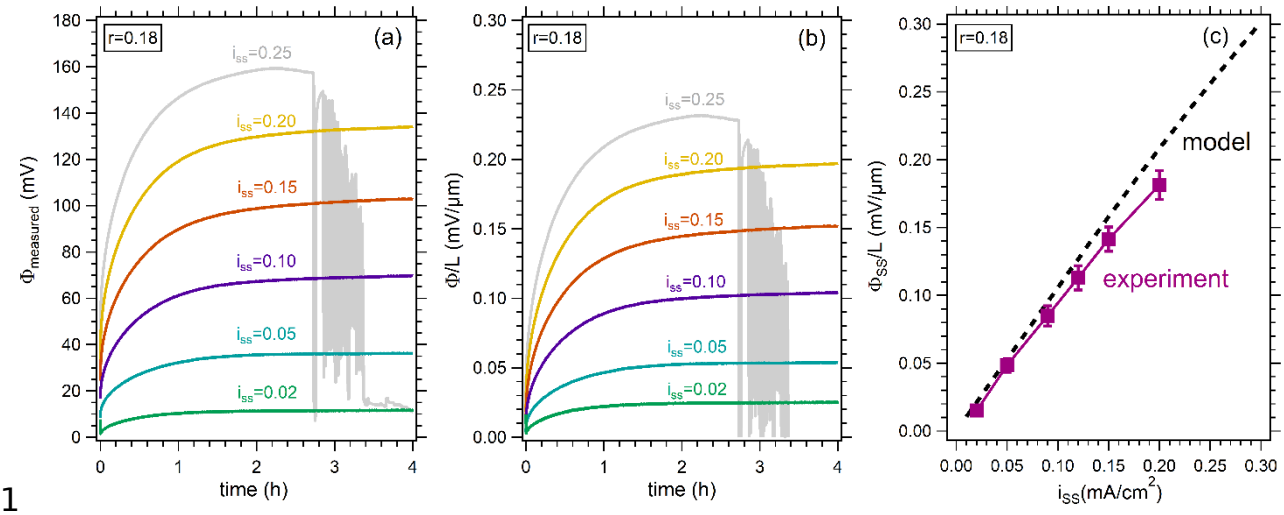

461

462**Figure 7. (a)** Time-dependent voltage profiles measured in r_{av}=0.18 at different
463steady-state current densities (i_{ss}=0.02 mA/cm^2 to i_{ss}=0.25 mA/cm^2). This cell failed
464at i_{ss}=0.25 mA/cm^2. **(b)** Same data as (a) with the interfacial impedance correction
465(eq. 26) and thickness normalization. **(c)** Comparison between predicted potential
466from model (dashed curve) and experimentally measured potential (markers) for
467r_{av}=0.18 at different current densities. The experimental measurements are carried
468out until cell failure, which is below the limiting current density predicted by the
469model.
470

In Figure 8 we compare Φ_{ss}/L over a wide range of salt concentrations, $0.01 \leq r_{av} \leq 0.3$, at a current density of $i_{ss} = 0.02$ mA/cm^2. The model results correspond to a system where $i_{ss}L = 0.001$ mA/cm; the concentration and potential profiles shown in Figure 3c and Figure 6c are thus applicable to the data shown in Figure 8. In spite of the fact that the concentration and potential profiles are approximately linear, Φ_{ss}/L is a complex function of salt concentration exhibiting two local minima at $r_{av} = 0.05$ and $r_{av} = 0.23$ (model predictions in Figure 8). The optimal salt concentration for battery applications would correspond to the case where Φ_{ss}/L is minimized; thus the local minima in Figure 8 are of practical significance. Local maxima in Φ_{ss}/L are observed at $r_{av} = 0.01$, $r_{av} = 0.15$, and $r_{av} = 0.3$. These maxima correspond to salt concentrations where D is small and t_+ is close zero or negative (see Table 1). At these concentrations, steep concentration gradients result in larger values of Φ_{ss}/L. The agreement between model predictions and experiments in Figure 8 is noteworthy.

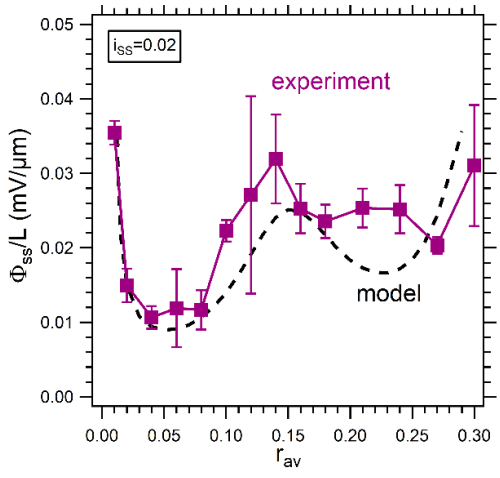

Figure 8. Comparison of predicted potential from model (dashed curve) and experimentally measured potential (markers) in PEO/LiTFSI electrolytes at i_{ss}=0.02 mA/cm^2.

We return to the time-dependent cycling curves shown in Figure 1. The complete data sets for r_{av} = 0.02 and r_{av} = 0.14 are shown in Figure 9. The solid yellow and blue curves in Figure 9 show averaged potential versus time data from r_{av} = 0.02 and r_{av} = 0.14, respectively, and the shaded regions signify the range of potentials obtained from three separate cells. The dashed curves in Figure 9 are transient model predictions obtained by numerically integrating eq. 15 – 20 using Comsol 5.3. We note that the transient model predictions are based on the same transport coefficients and thermodynamic factors (Table 2) as the steady-state model predictions shown in Figures 3, 4, and 6-8. It is evident from Figure 9 that the theoretical predictions are in good agreement with the time-dependent potential measurements made in lithium-polymer-lithium cells. Our model requires no adjustable parameters or simplifying assumptions. The agreement shown in Figure 9 justifies use of the model to explore current densities that could not be accessed experimentally due to dendrite growth.

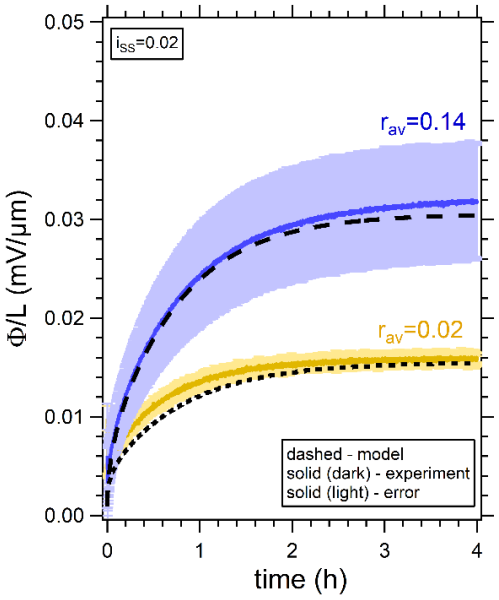

506

507**Figure 9.** Time-dependent potential curves for cells with r_{av} = 0.02 and r_{av} = 0.14
508polarized at i_{ss} = 0.02 mA/cm^2 from experiment (solid lines) and our transient model
509(dashed lines). The experimental data is an average from multiple lithium
510symmetric cells (dark solid curves), and the error is given by the standard deviation
511(light shaded area).

Conclusions

Using concentrated solution theory, we derive a set of equations that can be used to model salt concentration and potential profiles in symmetric lithium-polymer-lithium cells. Our theory, which accounts for the salt concentration dependence of the electrolyte transport properties and the thermodynamic factor, requires no adjustable parameters. First, we present a steady-state model, used to predict salt concentration and potential profiles in the electrolyte under the application of a steady dc current. Then we present a transient model, used to predict the time-dependence of potential in a symmetric cell during cycling.

Polymer electrolytes are convenient model systems to study ion transport due to the absence of convection. The transport properties of mixtures of polyethylene oxide (PEO) and lithium bis(trifluoromethanesulfonyl) imide (LiTFSI) salt have been previously reported over a wide range of salt concentrations, $0.01 \leq r \leq 0.3$, where $r = [Li^+]/[O]$.[21,22] We use these data as inputs for our model to predict concentration profiles, $r(x)$, and potential profiles, $\Phi(x)$ in PEO/LiTFSI electrolytes with varying current density, i_{ss}, thickness, L, and average electrolyte salt concentration, r_{av}. Both $r(x)$ and $\Phi(x)$ exhibit nonlinearities due to the strong concentration dependence of the transport and thermodynamic properties of the electrolyte; the steepest gradients occur at values of r where both the diffusion coefficient and the transference number exhibit minima. These calculations enable determination of the limiting

current density. Using our model, we calculate the steady-state potential, Φ_{ss}, across the symmetric cell as a function of r_{av} and i_{ss}. These calculations are compared with experimental data without resorting to any adjustable parameters. At low i_{ss}, we find excellent agreement between the values of Φ_{ss} predicted by the theory and those obtained experimentally in lithium-PEO/LiTFSI-lithium cells. Comparisons at higher i_{ss} are prohibited by the propensity of lithium dendrites to form in the experimental cells. The time-dependence of Φ obtained during cell cycling is consistent with predictions of the transient model, requiring no adjustable parameters or simplifying assumptions.

List of Symbols

PEO	polyethylene oxide
LiTFSI	lithium bis(trifluoromethanesulfonyl) imide
c	salt concentration (mol/cm^3)
c_0	solvent concentration (mol/cm^3)
c_T	total solution concentration (mol/cm^3)
D	salt diffusion coefficient (cm^2/s)
D	diffusion coefficient of the salt based on a thermodynamic driving
F	force (cm^2/s)
$f_\pm$	Faraday's constant (96485 C/mol)
i	mean molar activity of the salt
i_0	current density (mA/cm^2)
i_e	initial current density (mA/cm^2)
i_{limit}	exchange current density (mA/cm^2)
i_{ss}	limiting current density (mA/cm^2)
L	steady-state current density (mA/cm^2)
M_0	thickness of the electrolyte (µm)
m	molar mass of the solvent (g/mol)
Ne	molality (mol/kg)
N_-	dimensionless number defined by Equation 12
n	anion flux (mol/cm^2 s)
R	number of electrons
R_i	gas constant (J/mol K)
r	interfacial resistance (Ω cm^2)
r_{av}	moles of Li$^+$ per mole of ethylene oxide, [Li$^+$]/[O], local salt
T	concentration
Th	moles of Li$^+$ per mole of ethylene oxide, [Li$^+$]/[O], average salt
t	concentration
t_+	temperature (K)
$t_{+,ss}$	thermodynamic factor, equal to $1+d\ln\gamma_\pm/d\ln m$

t_-	time (h)
v	cation transference number
v_+, v_-	transference number obtained using stead-state current method
x	anion transference number
z_+, z_-	total number of ions into which the salt dissociates
	the number of cations and anions into which the salt dissociates
α_a, α_c	position (μm)
$\gamma_\pm$	charge number of cation and anion
μ_e	
μ_e^0	anodic and cathodic transfer coefficients
σ	mean molal activity coefficient of the salt
Φ	chemical potential of the electrolyte (J/mol)
Φ_0	chemical potential of the reference state (J/mol)
Φ_1	ionic conductivity (S/cm)
Φ_2	potential (mV)
$\Phi_{measured}$	initial potential (mV)
Φ_{ss}	potential of the electrode at electrode boundary (mV)
	potential of the electrolyte at electrode boundary (mV)
	measured cell potential (mV)
	steady-state potential (mV)

548

549

Acknowledgements

This work was intellectually led by the Joint Center for Energy Storage Research (JCESR), an Energy Innovation Hub funded by the U.S. Department of Energy (DOE), Office of Science, Basic Energy Sciences (BES), under Contract No. DEAC02-06CH11357.

Author Information

Corresponding Authors

*E-mail: nbalsara@berkeley.edu

Notes

The authors declare no competing financial interest.

References

(1) Lu, Y.; Tikekar, M.; Mohanty, R.; Hendrickson, K.; Ma, L.; Archer, L. A. Stable Cycling of Lithium Metal Batteries Using High Transference Number Electrolytes. *Adv. Energy Mater.* **2015**, *5* (9), 1402073.

(2) Stone, G. M.; Mullin, S. A.; Teran, A. A.; Hallinan, D. T.; Minor, A. M.; Hexemer, A.; Balsara, N. P. Resolution of the Modulus versus Adhesion Dilemma in Solid Polymer Electrolytes for Rechargeable Lithium Metal Batteries. *J. Electrochem. Soc.* **2012**, *159* (3), A222–A227.

(3) Lu, Y.; Tu, Z.; Archer, L. A. Stable lithium electrodeposition in liquid and nanoporous solid electrolytes. *Nat. Mater.* **2014**, *13* (10), 961–969.

(4) Qian, J.; Henderson, W. A.; Xu, W.; Bhattacharya, P.; Engelhard, M.; Borodin, O.; Zhang, J. G. High rate and stable cycling of lithium metal anode. *Nat. Commun.* **2015**.

(5) Appetecchi, G. B.; Scaccia, S.; Passerini, S. Investigation on the Stability of the Lithium-Polymer Electrolyte Interface. *J. Electrochem. Soc.* **2000**, *147* (12), 4448.

(6) Han, X.; Gong, Y.; Fu, K. (Kevin); He, X.; Hitz, G. T.; Dai, J.; Pearse, A.; Liu, B.; Wang, H.; Rubloff, G.; et al. Negating interfacial impedance in garnet-based solid-state Li metal batteries. *Nat. Mater.* **2016**, *16* (5), 572–579.

(7) Newman, J.; Thomas-Alyea, K. E. *Electrochemical Systems*, third.; John Wiley & Sons, 2004; Vol. 27.

(8) Thomas, K.; Newman, J.; Darling, R. Mathematical modeling of lithium batteries. In *Advances in Lithium-Ion Batteries*; 2002; pp 345–392.

(9) Doyle, M.; Newman, J.; Gozdz, A. S.; Schmutz, C. N.; Tarascon, J. Comparison of Modeling Predictions with Experimental Data from Plastic Lithium Ion Cells. *J. Electrochem. Soc.* **1996**, *143* (6), 1890.

(10) Doyle, M.; Fuller, T. F.; Newman, J. Modeling of Galvanostatic Charge and Discharge of the Lithium/Polymer/Insertion Cell. *J. Electrochem. Soc.* **1993**, *140* (6), 1526.

(11) Kim, U. S.; Shin, C. B.; Kim, C.-S. Modeling for the scale-up of a lithium-ion polymer battery. *J. Power Sources* **2009**, *189* (1), 841–846.

(12) Arora, P.; Doyle, M.; Gozdz, A. S.; White, R. E.; Newman, J. Comparison between computer simulations and experimental data for high-rate discharges of plastic lithium-ion batteries. *J. Power Sources* **2000**, *88* (2), 219–231.

(13) Srinivasan, V.; Newman, J. Discharge Model for the Lithium Iron-Phosphate Electrode. *J. Electrochem. Soc.* **2004**, *151* (10), A1517.

(14) Armand, M. B.; Chabagno, J. M.; Duclot, M. J. Poly-ethers as solid electrolytes. In *Fast Ion Transport in Solids, eds. Vashishta, P.M., Mundy, J.N., and Shenoy, G.K.*; North-Holland, 1979; pp 131–136.

(15) ARMAND, M. Polymer solid electrolytes - an overview. *Solid State Ionics* **1983**,

604 *9–10*, 745–754.

605(16) Meyer, W. H. Polymer Electrolytes for Lithium-Ion Batteries. *Adv. Mater.* **1998**,
606 *10* (6), 439–448.

607(17) Scrosati, B.; Vincent, C. A. Polymer Electrolytes: The Key to Lithium Polymer
608 Batteries. *MRS Bull.* **2011**, *25* (03), 28–30.

609(18) Liu, J.; Monroe, C. W. Solute-volume effects in electrolyte transport.
610 *Electrochim. Acta* **2014**, *135*, 447–460.

611(19) Ehrl, A.; Landesfeind, J.; Wall, W. A.; Gasteiger, H. A. Determination of
612 Transport Parameters in Liquid Binary Lithium Ion Battery Electrolytes. *J.*
613 *Electrochem. Soc.* **2017**, *164* (4), A826–A836.

614(20) Ehrl, A.; Landesfeind, J.; Wall, W. A.; Gasteiger, H. A. Determination of
615 Transport Parameters in Liquid Binary Electrolytes: Part II. Transference
616 Number. *J. Electrochem. Soc.* **2017**, *164* (12), A2716–A2731.

617(21) Pesko, D. M.; Timachova, K.; Bhattacharya, R.; Smith, M. C.; Villaluenga, I.;
618 Newman, J.; Balsara, N. P. Negative Transference Numbers in Poly(ethylene
619 oxide)-Based Electrolytes. *J. Electrochem. Soc.* **2017**, *164* (11), E3569–E3575.

620(22) Villaluenga, I.; Pesko, D.; Timachova, K.; Feng, Z.; Newman, J.; Srinivasan, V.;
621 Balsara, N. Negative Stefan-Maxwell Diffusion Coefficients and Complete
622 Electrochemical Transport Characterization of Homopolymer and Block
623 Copolymer Electrolytes. *J. Electrochem. Soc.* **2018**.

624(23) Balsara, N. P.; Newman, J. Relationship between Steady-State Current in
625 Symmetric Cells and Transference Number of Electrolytes Comprising
626 Univalent and Multivalent Ions. *J. Electrochem. Soc.* **2015**, *162* (14), A2720–
627 A2722.

628(24) Wu, S.-L.; Javier, A. E.; Devaux, D.; Balsara, N. P.; Srinivasan, V. Discharge
629 Characteristics of Lithium Battery Electrodes with a Semiconducting Polymer
630 Studied by Continuum Modeling and Experiment. *J. Electrochem. Soc.* **2014**,
631 *161* (12), A1836–A1843.

632(25) Zheng, Q.; Pesko, D. M.; Savoie, B. M.; Timachova, K.; Hasan, A. L.; Smith, M.
633 C.; Miller, T. F.; Coates, G. W.; Balsara, N. P. Optimizing Ion Transport in
634 Polyether-Based Electrolytes for Lithium Batteries. *Macromolecules* **2018**, *51*
635 (8).

636(26) Newman, J.; Tiedemann, W. Porous-electrode theory with battery applications.
637 *AIChE J.* **1975**, *21* (1), 25–41.

638(27) Fuller, T. F.; Doyle, M.; Newman, J. Simulation and Optimization of the Dual
639 Lithium Ion Insertion Cell. *J. Electrochem. Soc.* **1994**, *141* (1), 1.

640

641